

Anatomy of the spin Hall effect in ferromagnetic metals

Fanxing Zheng , Meng Zhu, Jianting Dong, Xinlu Li, Ye Zhou, Kun Wu, and Jia Zhang*

School of Physics and Wuhan National High Magnetic Field Center, Huazhong University of Science and Technology, 430074 Wuhan, China



(Received 1 November 2023; revised 16 April 2024; accepted 3 May 2024; published 3 June 2024)

The spin Hall effect (SHE) is one of the most important spin-to-charge conversion mechanisms in spintronics and has been intensively investigated in nonmagnetic materials. However, the SHE in ferromagnetic metals has been rarely studied and remains obscure. Here, we clarify that the SHE in ferromagnetic metals can be classified into three categories including conventional-, spin anomalous-, and magnetic spin Hall effect. By using first-principles calculations, we find the above three spin Hall mechanisms do coexist in common ferromagnetic metals. Particularly, for Pt-based ferromagnetic alloys, comparable conventional and magnetic spin Hall angles have been predicted. In addition, we investigate the temperature dependence and scaling behavior of different types of spin Hall conductivity by taking into account the lattice vibration and spin disorder scattering. Finally, we argue that ferromagnetic metals with remarkable unconventional SHE may be efficient spin current sources with out-of-plane spin polarization for spin-orbit torque-induced switching and spin terahertz emission. This work provides a comprehensive understanding of the SHE in ferromagnetic metals and may pave the way for promising applications in spin-to-charge conversion spintronics devices.

DOI: [10.1103/PhysRevB.109.224401](https://doi.org/10.1103/PhysRevB.109.224401)

I. INTRODUCTION

In nonmagnetic materials, the conventional spin Hall effect (CSHE) originates from the asymmetric deflection of electrons with opposite spin in the presence of spin-orbit coupling when charge flows [1]. A transverse spin current with the spin polarization perpendicular to the plane of charge and spin current will be generated by spin Hall effect (SHE), which can be described as $\mathbf{J}_s = \theta_{\text{CSH}}(\hbar/2e)\mathbf{J}_c \times \hat{S}$, where θ_{CSH} is the conventional spin Hall angle, \mathbf{J}_c is charge current density, \hat{S} is the spin-polarization direction, \hbar is the reduced Planck constant, and e is the elementary charge. CSHE and inverse CSHE in nonmagnetic heavy metals like Pt, Ta, W, and alloys have been intensively studied for spin-to-charge conversion in spintronics [2]. Especially, in “heavy-metal–ferromagnet” bilayer, a charge current in heavy metal produces spin current through CSHE mechanism and generates spin-orbit torque (SOT) on adjacent ferromagnets (CSHE-SOT), leading to magnetization switching [3–5]. The CSHE-SOT provides an efficient writing scheme for the next-generation magnetic random access memory [6]. However, the charge current, spin current, and its spin polarization generated by CSHE must be mutually orthogonal, which has largely impeded its efficiency.

Conventional spin Hall was first experimentally discovered in ferromagnetic permalloy [7], which was found to be magnetization independent. The spin current associated with anomalous Hall effect [8] in ferromagnets was proposed later, known as spin anomalous Hall effect (SAHE) [9]. Subsequent experiments have demonstrated that the spin current generated by SAHE can also exert an SOT on ferromagnets [10,11], and if sufficiently strong, it will be able to switch the magnetization [12–15]. Recently, SAHE in ferromagnets Fe, Co, Ni, and L10-(Fe, Co, Ni)Pt has been investigated by

first-principles calculations [16,17]. Imposed by magnetic point-group symmetry [18], there is a third type of SHE called magnetic spin Hall effect (MSHE) in ferromagnetic metals [19–21]. The MSHE was first experimentally observed in noncollinear antiferromagnet Mn_3Sn [22], and theoretically investigated in Fe, Co, Ni [21].

The features of the spin current generated by different spin Hall mechanisms in practical ferromagnetic metals still remain unclear and have been ignored in spin Hall experiments for a long time. In this work, using first-principles calculations we investigate the SHE in representative ferromagnetic alloys including (Fe, Co, Ni)Pt, NiFe, and CoFe. We first clarify and analyze the different SHE mechanisms in ferromagnetic metals. Then, the spin Hall conductivity and spin Hall angle are evaluated based on the Kubo-Bastin linear response formalism [23]. Our results indicate that the Pt-based ferromagnetic alloys exhibit a significant conventional and magnetic spin Hall effect, comparable to that of pure Pt. Furthermore, we analyze the finite-temperature transport properties by considering phonon- and spin-disorder scattering, and derive the scaling behavior of spin Hall conductivity. Finally, we discuss the perspective applications of SHE in ferromagnetic metals including the field-free switching of perpendicular magnetization by SOT and spin terahertz (THz) emission.

II. THEORY METHODS

A. Calculation details

The first-principles calculations were performed by using fully relativistic multiple scattering Korringa-Kohn-Rostoker (KKR) Green’s function method [24,25]. The cutoff $l_{\text{max}} = 3$ was used for the angular momentum expansion of Green’s function. For the self-consistent calculations the Vosko-Wilk-Nussair parametrization was employed for the exchange-correction potential in the local density approximation [26].

*jiazhang@hust.edu.cn

The involved energy integration was performed on a semi-circle in the complex plane by using 50 energy points and $45 \times 45 \times 45$ k points in the Brillouin zone (BZ). Using these self-consistent field potentials, the spin Hall conductivity was calculated based on the Kubo-Bastin linear response formalism [23]; approximately 10^7 k points in the BZ were found to be sufficient for convergence of spin Hall conductivity. The finite-temperature effects were treated within the so-called alloy analogy model based on the coherent potential approximation theory [27–29].

In Cartesian coordinates, the linearly responsive spin current propagates along the μ axis with spin polarization in the ξ direction stimulated by electric field in the ν axis, and can be expressed as

$$J_{\mu}^{\xi} = \sum_{\nu} J_{\mu\nu}^{\xi} = \sum_{\nu} \sigma_{\mu\nu}^{\xi} E_{\nu} (\mu, \nu, \xi \in \{x, y, z\}). \quad (1)$$

The spin Hall conductivity $\sigma_{\mu\nu}^{\xi}$ is a third-rank tensor and can be evaluated from Green's function based on Kubo-Bastin formalism [23]. For alloy, we perform two separate calculations with and without vertex correction. The calculated conductivity with vertex correction (VC) contains both intrinsic and extrinsic contribution, while the conductivity without vertex correction (NVC) contains only intrinsic contribution. Therefore, the intrinsic and extrinsic spin Hall conductivity can be obtained by $\sigma^{\text{intr}} = \sigma^{\text{NVC}}$, and $\sigma^{\text{extr}} = \sigma^{\text{VC}} - \sigma^{\text{NVC}}$. Our calculations indicate the dominant intrinsic contributions of SHE in ferromagnetic metals (see Appendix A) [23,30]. The spin current calculated in this work accounts only for the conventional bulk component and neglects the spin torque that is quadratic in spin-orbit coupling (SOC) strength and as a higher-order correction to the spin Hall effect [31–33].

B. Symmetry analysis

The A1 phase of (Fe, Co, Ni)₅₀Pt₅₀ alloy in fcc crystal structure belongs to the magnetic Laue group $4/\text{mm}'\text{m}'$. The direction of magnetic moment \mathbf{M} has been set to be along the x direction in our calculations. Thus, the symmetry-imposed spin conductivity tensor can be written as [18]

$$\begin{aligned} \sigma_{\mu\nu}^x &= \begin{pmatrix} \sigma_{xx}^x & 0 & 0 \\ 0 & \sigma_{yy}^x & \sigma_{yz}^x \\ 0 & \sigma_{zy}^x & \sigma_{zz}^x \end{pmatrix} \\ \sigma_{\mu\nu}^y &= \begin{pmatrix} 0 & \sigma_{xy}^y & \sigma_{xz}^y \\ \sigma_{yx}^y & 0 & 0 \\ \sigma_{zx}^y & 0 & 0 \end{pmatrix} \\ \sigma_{\mu\nu}^z &= \begin{pmatrix} 0 & \sigma_{xy}^z & \sigma_{xz}^z \\ \sigma_{yx}^z & 0 & 0 \\ \sigma_{zx}^z & 0 & 0 \end{pmatrix}. \end{aligned} \quad (2)$$

The diagonal elements σ_{xx}^x , σ_{yy}^y , and σ_{zz}^z are trivial and describe the spin-polarized longitudinal conductivity in ferromagnetic metals. The off-diagonal elements $\sigma_{\mu\nu}^{\xi}$ are spin Hall conductivities and can be classified into three spin Hall mechanisms, *i.e.*, CSHE, MSHE, and SAHE.

By taking Fe₅₀Pt₅₀ as an example, the classification of spin Hall conductivities and the schematic diagram of spin current are shown in Table I. The elements of $\sigma_{\mu\nu}^{\xi}$ with Levi-Civita symbol $\varepsilon_{\mu\nu\xi} \neq 0$ indicate the charge current, spin current,

and spin polarization are mutually orthogonal. Those elements are even with respect to time-reversal operation (T -even), *i.e.*, $\sigma_{\mu\nu}^{\xi}(\mathbf{M}) = \sigma_{\mu\nu}^{\xi}(-\mathbf{M})$. Among them, σ_{yx}^z , σ_{zx}^y , σ_{xy}^z , and σ_{xz}^y can be exclusively attributed to CSHE contribution. Notably, σ_{yx}^z and σ_{xy}^z are not identical in ferromagnetic metals due to the lower symmetry in the presence of magnetic moment and SOC.

The other two elements σ_{zy}^x and σ_{yz}^x contain contributions from CSHE as well as SAHE since now the spin current propagates along the $\hat{m} \times \mathbf{J}_c$ direction. Thus, the element only corresponding to SAHE, *i.e.*, spin anomalous Hall conductivity (σ_{SAH}), can be obtained by

$$\begin{aligned} \sigma_{\text{SAH}} &= \sigma_{yx}^z(\hat{m}|\hat{z}; \text{CSHE} + \text{SAHE}) - \sigma_{yx}^z(\hat{m}|\hat{x}; \text{CSHE}) \\ &= \sigma_{zy}^x(\hat{m}|\hat{x}) - \sigma_{yz}^x(\hat{m}|\hat{x}). \end{aligned} \quad (3)$$

The remaining four elements σ_{xy}^y , σ_{yx}^y , σ_{xz}^z , and σ_{zx}^z can be attributed to MSHE. They are odd respecting time-reversal operation (T -odd), *i.e.*, $\sigma_{\mu\nu}^{\xi}(\mathbf{M}) = -\sigma_{\mu\nu}^{\xi}(-\mathbf{M})$. It is worth pointing out that for MSHE, the charge current, spin current, and spin polarization are not mutually orthogonal. Instead, two of them can be parallel to each other. As shown in Table I, the spin current corresponding to σ_{zx}^z (σ_{yx}^y) exhibits the spin polarization parallel to the spin current propagation direction, while the spin current corresponding to σ_{xz}^z (σ_{xy}^y) has the spin polarization aligned with the direction of the charge current. From this perspective, the spin current generated by MSHE could break the restriction on spin polarization by CSHE and SAHE mechanisms and extend its potential applications for emergent spin-to-charge conversion phenomena as we will discuss later.

For ferromagnetic Fe₅₀Pt₅₀ alloy, the conventional spin Hall and magnetic spin Hall conductivities have similar magnitude, indicating the coexistence of dominant CSHE and MSHE mechanisms in FePt alloy. Although the absolute value of conventional spin Hall and magnetic spin Hall conductivity for Fe₅₀Pt₅₀ is around a one-quarter of the spin Hall conductivity in Pt ($4336 \hbar/2e(\Omega \text{ cm})^{-1}$ in our calculation), Fe₅₀Pt₅₀ has comparable spin Hall angle as Pt due to its relatively lower longitudinal conductivity.

III. RESULTS AND DISCUSSION

A. SHE for different FM alloys

In order to obtain a universal understanding on SHE in practical ferromagnetic metals, we calculate the spin Hall conductivity and evaluate the spin Hall angle for (Fe, Co, Ni)₅₀Pt₅₀, Ni₈₀Fe₂₀, and Co₅₀Fe₅₀ alloys. For each alloy, the calculated longitudinal conductivity σ_{xx} and spin Hall conductivities in comparison with typical nonmagnets, antiferromagnets, and magnets can be found in Tables II and III attached in Appendix B. Here, we use the representative elements σ_{yx}^z and σ_{zx}^z to denote the conventional (σ_{CSH}) and magnetic spin Hall conductivities (σ_{MSH}); the definition of spin anomalous Hall conductivity (σ_{SAH}) has been given above. Thus, the spin Hall angles for CSHE, SAHE, and MSHE can be defined by the characteristic spin Hall conductivity as $\theta_{\text{CSH}} = \sigma_{\text{CSH}}/\sigma_{xx}$, $\theta_{\text{SAH}} = \sigma_{\text{SAH}}/\sigma_{xx}$, $\theta_{\text{MSH}} = \sigma_{\text{MSH}}/\sigma_{xx}$ and the results are shown in Fig. 1. It can be seen that the conventional spin Hall angle θ_{CSH} for Fe₅₀Pt₅₀

TABLE I. Classification of SHE in Fe₅₀Pt₅₀. The calculated spin Hall conductivities (unit: $\hbar/2e(\Omega \cdot \text{cm})^{-1}$) for A1 phase Fe₅₀Pt₅₀ (the conductivities in the parentheses can be obtained by symmetry operation) and the schematic diagram of spin current generated by CSHE, SAHE, and MSHE, where the green and blue arrows indicate the directions of charge current J_c and magnetization M . The black and red arrows represent the directions of spin current J_s and the spin polarization S .

Classification of SHE	Spin Hall conductivity		Direction relationship	Schematic diagram
CSHE (T -even)	$\sigma_{yx}^z (-\sigma_{zx}^y)$	1195	$J_c // M$ $S \perp J_s \perp J_c$	
	$\sigma_{xy}^z (-\sigma_{xz}^y)$	-1073	$J_c \perp M$ $S \perp J_s \perp J_c$	
SAHE+CSHE (T -even)	$\sigma_{zy}^x (-\sigma_{yz}^x)$	1354	$J_c \perp M$ $S \perp J_s \perp J_c$	
MSHE (T -odd)	$\sigma_{zx}^z (\sigma_{yx}^y)$	788	$J_c // M$ $S // J_s \perp J_c$	
	$\sigma_{xy}^y (\sigma_{xz}^z)$	-657	$J_c \perp M$ $S // J_c \perp J_s$	

($\theta_{\text{CSH}}^{\text{Fe}_{50}\text{Pt}_{50}} = 0.065$) and Co₅₀Pt₅₀ ($\theta_{\text{CSH}}^{\text{Co}_{50}\text{Pt}_{50}} = 0.071$) alloys are comparable to that of Pt ($\theta_{\text{CSH}}^{\text{Pt}} = 0.08 \pm 0.02$ from experiment [3]). In addition, the magnetic spin Hall angles θ_{MSH} for Pt-based alloys are also sizable ($\theta_{\text{MSH}}^{\text{Fe}_{50}\text{Pt}_{50}} = 0.044$, $\theta_{\text{MSH}}^{\text{Co}_{50}\text{Pt}_{50}} =$

0.043 , and $\theta_{\text{MSH}}^{\text{Ni}_{50}\text{Pt}_{50}} = -0.032$), which are in the same order of magnitude as θ_{CSH} . The relative magnitude of spin Hall angles and the main spin Hall mechanism in ferromagnetic metals depend on specific materials. For example, the leading spin Hall mechanism in Fe₅₀Pt₅₀ and Co₅₀Pt₅₀ is CSHE, followed by MSHE, and the SAHE is the smallest, while for Ni₅₀Pt₅₀ the relative values of spin Hall angle are $\theta_{\text{MSH}} > \theta_{\text{CSH}} > \theta_{\text{SAH}}$. Interestingly, the spin Hall angles in typical 3d ferromagnetic metals are also pronounced. For Ni₈₀Fe₂₀, it has comparable values of θ_{CSH} and θ_{SAH} but small θ_{MSH} , while for Co₅₀Fe₅₀ the θ_{MSH} is the largest.

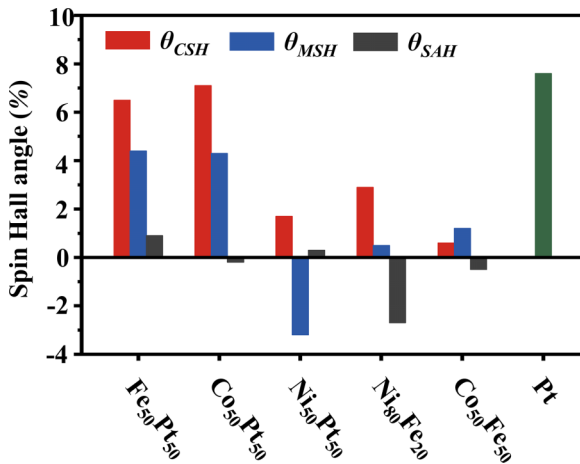


FIG. 1. The spin Hall angles corresponding to CSHE (θ_{CSH}), MSHE (θ_{MSH}), and SAHE (θ_{SAH}) for (Fe, Co, Ni)₅₀Pt₅₀, Ni₈₀Fe₂₀, and Co₅₀Fe₅₀ alloys. The green column indicates the conventional spin Hall angle for Pt as reference.

B. Alloy composition dependence on SHE

The relative strength of SHE can also be optimized by varying the composition of ferromagnetic alloy. Figure 2(a) shows the spin Hall angles as a function of Fe composition in FePt alloy. One can find the conventional spin Hall angle decreases monotonically by around a factor of 8 with increasing Fe concentration. Similar behavior also appears in spin anomalous Hall angle but with less decreasing tendency. In contrast, the magnetic spin Hall angle does not show significant change ranging between 0.03 to 0.045 with increasing Fe concentration in FePt alloy.

With the Fe concentration increasing in FePt alloy, various spin Hall related electronic structure properties change, such

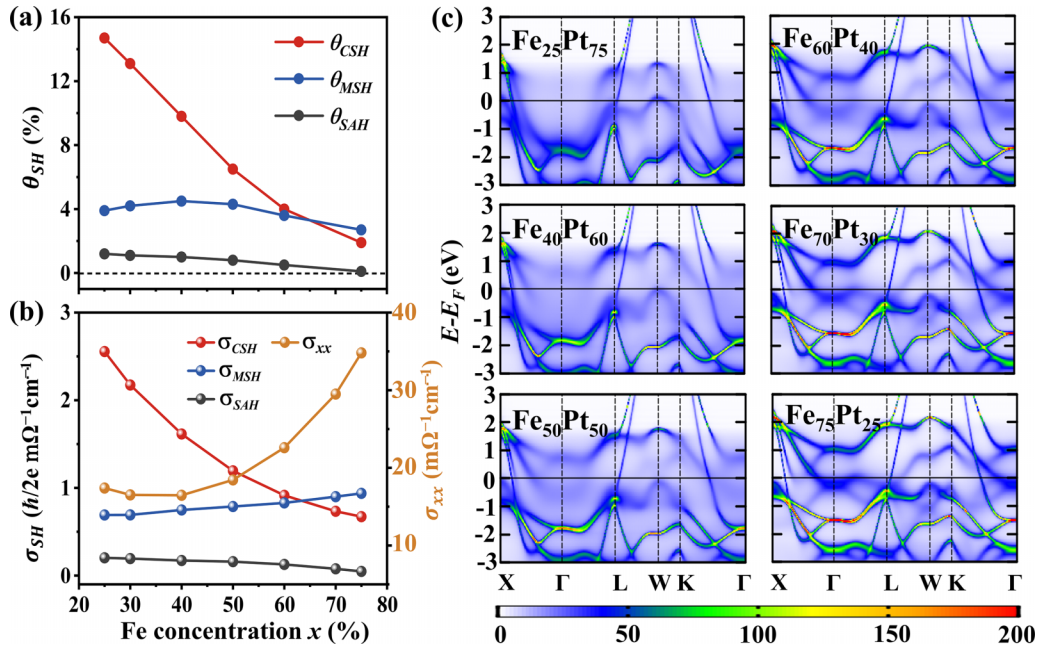


FIG. 2. (a) The conventional, spin anomalous, and magnetic spin Hall angles and (b) The spin Hall and longitudinal conductivity as a function of Fe composition in Fe_xPt_{100-x} alloys. The conductivity refers to the right axis. (c) The Bloch spectra of FePt alloy with increasing Fe composition.

as band-energy broadening, spin-orbit coupling strength, etc. Before analyzing the composition dependence of spin Hall effect in FePt alloy, we first adopt magnetic Rashba models to derive analytical expressions on spin Hall conductivity and try to understand the general features of various spin Hall mechanisms in magnetic systems (see Appendix C). In Rashba models, the conventional and spin anomalous Hall conductivity can be calculated in the clean limit, i.e., the band-energy broadening $\hbar\Gamma \rightarrow 0$, which turns into the summation of spin Berry curvature in the Brillouin zone. Therefore, both the conventional and spin anomalous Hall conductivity show no explicit dependence on Γ . In contrast, to evaluate magnetic spin Hall conductivity and longitudinal conductivity, a constant energy broadening $\hbar\Gamma$ must be taken into account, and both of them are inversely proportional to Γ . We now try to qualitatively understand the different dependency of spin Hall effect on FePt alloy composition. As one can see in Fig. 2(c), when the Fe composition increases, generally the band-energy broadening around Fermi energy decreases, which leads to the increase of σ_{MSH} and σ_{xx} as shown in Fig. 2(b). Meanwhile, the magnetic spin Hall angle does not show obvious dependence on alloy composition as shown in Fig. 2(a). On the other hand, conventional and spin anomalous Hall conductivity are more susceptible to the SOC strength (see Appendix D for the dependence of various spin Hall effect on SOC strength). Thus, with larger Fe composition in FePt alloy, it results in weaker average SOC strength and the decreasing of σ_{CSH} and σ_{SAH} as shown in Fig. 2(b).

C. Temperature dependence and scaling behavior of SHE

To further have an in-depth understanding on SHE in ferromagnetic metals, we separately consider two dominat-

ing scattering mechanisms at finite temperatures, namely magnetization-independent lattice vibration (phonon) scattering and magnetization-dependent spin disorder scattering. We calculate the spin Hall conductivity of $Fe_{50}Pt_{50}$ alloy in the presence of the above two scattering mechanisms by employing the alloy analogy model [34]. Figure 3(a) shows the calculated longitudinal electrical resistivity ρ_{xx} of $Fe_{50}Pt_{50}$ as a function of temperature, where ρ^{ph} and ρ^{mag} are the resistivity corresponding to phonon and spin disorder scattering, respectively. Similar to common ferromagnetic metals, ρ^{ph} of $Fe_{50}Pt_{50}$ is linearly proportional to temperature (T) when T is larger than its Debye temperature (325 K). ρ^{mag} can be well described as $\rho^{mag} = \rho^{para}\{1 - [M(T)/M_0]^2\}$, and approaches to constant paramagnetic resistivity ρ^{para} above Curie temperature T_c .

The temperature-dependent spin Hall conductivity of $Fe_{50}Pt_{50}$ is shown in Fig. 3(b). When only phonon scattering is considered, all three types of spin Hall conductivities show linear dependence on temperature. However, in the presence of spin disorder scattering, the conventional spin Hall conductivity first decreases with increasing temperature and then remains constant when T is above T_c . In contrast, both magnetic and spin anomalous conductivity vanish when $Fe_{50}Pt_{50}$ alloy becomes paramagnetic ($T > T_c$), which confirms that the presence of magnetic order is necessary to have nonzero magnetic and spin anomalous conductivity.

We then discuss the scaling behavior of spin Hall conductivity with longitudinal conductivity σ_{xx} . As shown in Fig. 3(c), in the conductivity range of phonon scattering, the spin Hall conductivities can be linearly scaled as $\sigma_{SH} \sim a\sigma_{xx} + b$, with different a and b parameters for CSHE, MSHE, and SAHE. It is also worth noting that in this conductivity range, the spin Hall conductivities fall into the same curve regard-

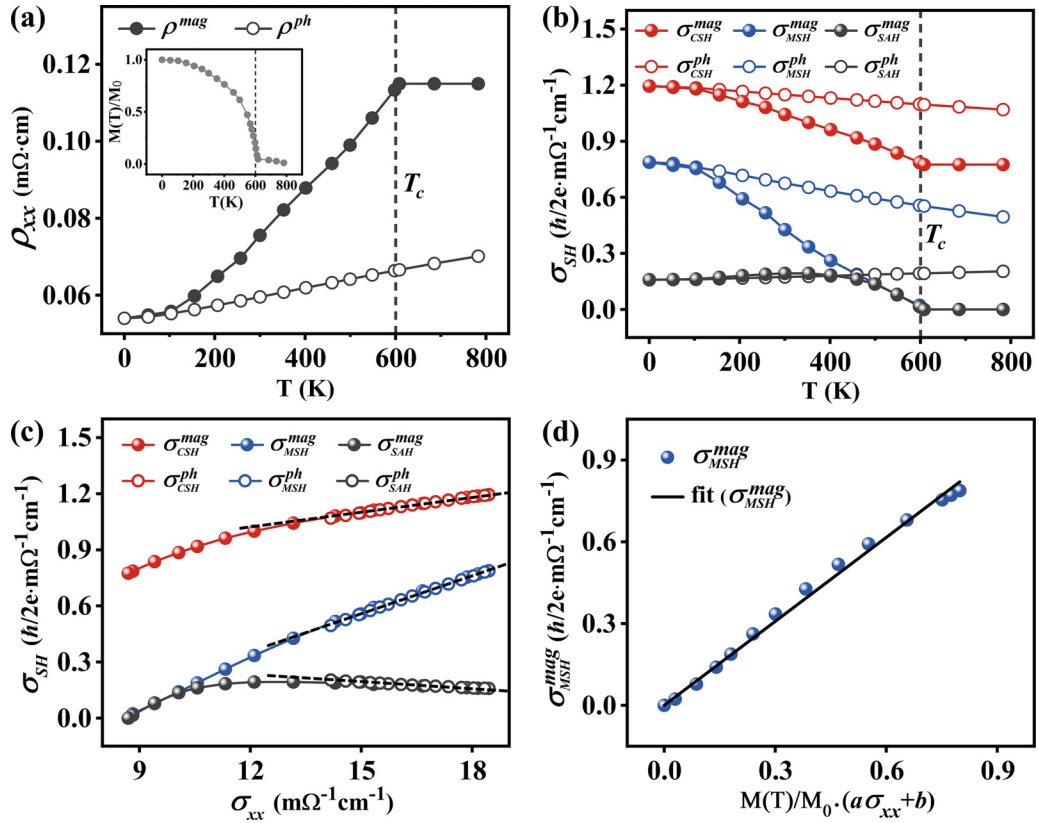


FIG. 3. (a) The temperature dependence of electrical resistivity and (b) spin Hall conductivity for Fe₅₀Pt₅₀ alloy. The inset in (a) shows the experimental $M(T)$ curve we adopted in the spin disorder scattering calculations. The terms with superscript “mag” and “ph” represent the quantities corresponding to spin disorder and lattice vibration, respectively. (c) The calculated spin Hall conductivity as a function of longitudinal conductivity σ_{xx} , where the black dashed line indicates the linear fit with $\sigma_{SH} \sim a\sigma_{xx} + b$. (d) The calculated σ_{MSH}^{mag} and the fitting curve.

less of phonon- or spin disorder scattering, which suggests that temperature-dependent magnetization does not have significant impact on spin Hall conductivity in this region. In the lower-conductivity region which can only be reached by considering spin disorder scattering, the spin Hall conductivities deviate from linear dependence on σ_{xx} . For instance, the conventional spin Hall conductivity now has quadratic term on σ_{xx} , while the magnetic and spin anomalous Hall conductivities are also dependent on magnetization $M(T)/M_0$. Especially as shown in Fig. 3(d), the magnetic spin Hall conductivity is found to be proportional to the magnetization $M(T)$ and can be scaled by $\sigma_{MSH}^{mag} \sim M(T)/M_0(a\sigma_{xx} + b)$, where a and b are the linearly fitting parameters from the above phonon-scattering conductivity region.

D. Practical application of multi-SHE

Finally, we focus on the practical application of the co-existing multi-SHE mechanisms in ferromagnetic metals. As shown in Fig. 4(a), if the electric current is applied along the x direction in (001)-oriented FePt film and the magnetization \mathbf{M} can rotate in xy plane by magnetic field, when the magnetization is set to be perpendicular to the charge current \mathbf{J}_c , the spin current \mathbf{J}_s along the z axis will be produced by CSHE and SAHE with spin-polarization \mathbf{S} only having y component.

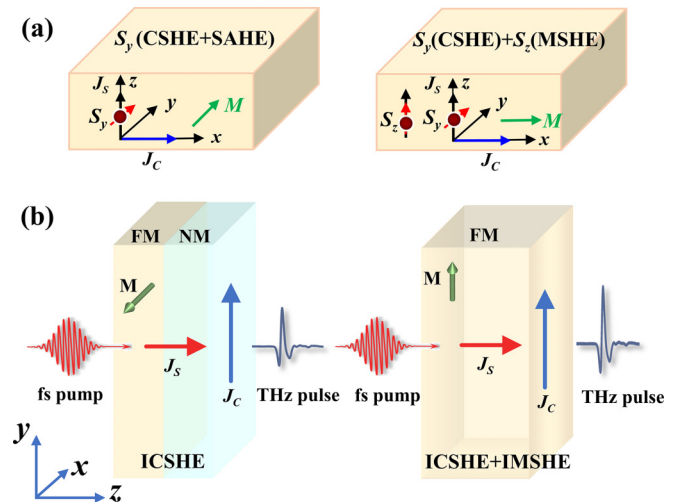


FIG. 4. (a) Illustrations of ferromagnetic metals being used as spin current source for SOT switching. The directions of charge current, the magnetization, and spin current have been marked with blue, green, and black arrows, respectively. The spin-polarization \mathbf{S} of the spin current has been shown in red arrow. (Left) The magnetization \mathbf{M} is perpendicular to \mathbf{J}_c . (Right) The magnetization \mathbf{M} is parallel to \mathbf{J}_c . (b) Schematic of THz emission in FM/NM structure (Left) and single FM layer (Right) with synergetic spin Hall mechanisms.

In contrast, when the magnetization is set to be parallel to the charge current \mathbf{J}_c , the spin current \mathbf{J}_s with spin-polarization \mathbf{S} have both y and z components originating from CSHE and MSHE mechanism, respectively. Importantly, the spin-polarization component S_z is desirable for field-free switching of perpendicularly magnetized free layer by SHE-SOT mechanism [5], which cannot be acquired in nonmagnetic heavy metals Pt, Ta, etc. Depending on the direction of in-plane magnetization direction \hat{m} , the spin-polarization \mathbf{S} of the spin current propagates along the z axis and can be described as

$$\vec{S} = \theta_{\text{CSH}}\hat{y} + \theta_{\text{SAH}}(\hat{m} \cdot \hat{y})\hat{m} + \theta_{\text{MSH}}(\hat{m} \cdot \hat{x})\hat{z} \quad (4)$$

A recent experiment indeed demonstrates the efficient field-free switching of perpendicular magnetization by taking advantage of the multiple spin polarization of spin current generated by SHE in ferromagnetic metals [35]. There is also experiment confirming that the ferromagnet can generate spin current with spin polarization noncollinear to its magnetization and the transverse spin component can be protected from dephasing [36]. In addition, as shown in Fig. 4(b), the spin terahertz (THz) emission has been widely studied in ferromagnet/nonmagnet bilayers, in which the spin current generated in ferromagnet will be converted to THz charge current in nonmagnetic heavy-metal layer via the inverse spin Hall effect [37–39]. Due to the elimination of interfacial backflow as in bilayer, the spin-to-charge conversion and the spin THz emission in ferromagnetic single layer like FePt alloy with prominent spin Hall effect will be greatly enhanced (see Appendix E for spin THz emission in single ferromagnetic layer). On the other hand, in ferromagnetic single layer it allows for spin-to-charge conversion via synergistic spin Hall mechanisms, which will further enhance THz emission.

IV. CONCLUSION

In summary, we have investigated all types of spin Hall effect which coexisted in ferromagnetic metals and classified them into CSHE, MSHE, and SAHE. By using first-principles calculation, we explicitly evaluated the spin Hall conductivity and spin Hall angle corresponding to the three types of SHE for practical ferromagnetic alloys. The calculations unveiled the large conventional and magnetic spin Hall angle appeared in Pt-based alloys, comparable to that of nonmagnetic heavy metals. The presence of remarkable unconventional SHE in ferromagnetic metal makes them an efficient spin current source with out-of-plane spin polarization for SOT-induced switching and spin THz emission. Furthermore, we have investigated the finite-temperature transport properties by considering phonon- and spin disorder scattering, and derived the scaling behavior of SHE. Our results provide a comprehensive understanding and highlight the significance

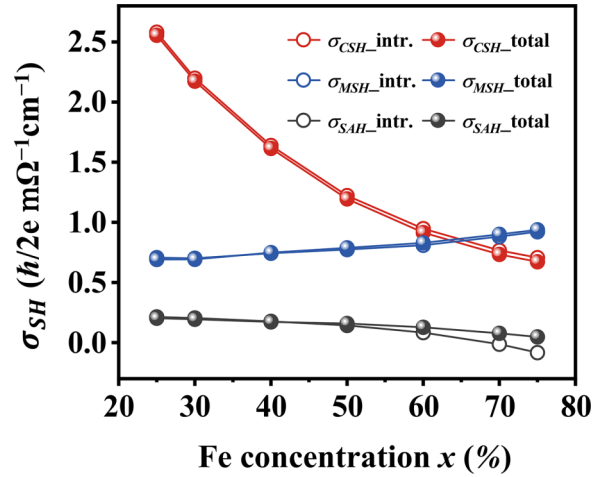


FIG. 5. The spin Hall conductivity for the $\text{Fe}_x\text{Pt}_{100-x}$ ($20 < x < 80$) alloys. The red, blue, and black lines are corresponding to conventional, magnetic, and spin anomalous Hall conductivities. The hollow circle represents the intrinsic contribution, and solid circle indicates the total contributions including both intrinsic and extrinsic contributions.

of the SHE in ferromagnetic metals, which may promote the future research progress on ferromagnet-based spin-to-charge conversion in spintronics.

ACKNOWLEDGMENT

This work was supported by the National Natural Science Foundation of China (Grant No. 12174129), and the open research fund of Beijing National Laboratory for Condensed Matter Physics (Grant No. 2023BNLCPKF010).

APPENDIX A: THE INTRINSIC AND EXTRINSIC SPIN HALL CONDUCTIVITY FOR $\text{Fe}_x\text{Pt}_{100-x}$ ALLOY

To further analyze the intrinsic and extrinsic contributions, we perform two separate calculations with and without vertex correction. The calculated conductivity with vertex correction (VC) contains both intrinsic and extrinsic contribution, i.e., σ_{total} , while the conductivity without vertex correction (NVC) contains only intrinsic contribution, i.e., $\sigma_{\text{intr.}}$. As shown in Fig. 5, our calculations indicate the dominant intrinsic contributions of SHE in ferromagnetic metals (See Fig. 5).

APPENDIX B: THE SPIN HALL CONDUCTIVITY AND LONGITUDINAL CONDUCTIVITY σ_{xx} FOR FM ALLOYS

For each alloy, the calculated longitudinal conductivity σ_{xx} and spin Hall conductivities are listed in Table II. And the spin Hall conductivities in comparison with typical nonmagnets, antiferromagnets, and magnets are shown in Table III, one can notice that the significant magnetic spin Hall conductivity exists in A1 FePt alloy, which will make it as an efficient spin current source with out-of-plane spin polarization.

TABLE II. The calculated spin Hall conductivity components (unit: $\hbar/2e(\Omega \cdot \text{cm})^{-1}$) and the longitudinal conductivity σ_{xx} (unit: $(\Omega \cdot \text{cm})^{-1}$), the available calculated and experimental values are also listed for reference) of (Fe, Co, Ni)₅₀Pt₅₀, Ni₈₀Fe₂₀, and Co₅₀Fe₅₀ alloys.

	$\sigma_{\mu\nu}^{\xi}$	Fe ₅₀ Pt ₅₀	Co ₅₀ Pt ₅₀	Ni ₅₀ Pt ₅₀	Ni ₈₀ Fe ₂₀	Co ₅₀ Fe ₅₀
CSHE	$\sigma_{yx}^z(-\sigma_{zx}^y)$	1195	2039	2315	12446	1802
(<i>T</i> -even)	$\sigma_{xy}^z(-\sigma_{xz}^y)$	-1 073	-1897	-566	-12682	-2139
SAHE+SHE	$\sigma_{zy}^x(-\sigma_{yz}^x)$	1354	1993	2755	989	260
(<i>T</i> -even)						
MSHE	$\sigma_{zx}^z(\sigma_{yx}^y)$	788	1222	-4513	1904	3720
(<i>T</i> -odd)	$\sigma_{xy}^y(\sigma_{xz}^z)$	-657	-932	4277	-5106	-4221
Longitudinal	σ_{xx}	18452	28675	139375	421537	302776
conductivity	σ_{xx}^{ref}	13513 [40]	34482 [41]		452488 [43]	
		18867 [40]	23557 [42]		238095 [44]	

TABLE III. The spin Hall conductivities (unit: $\hbar/2e(\Omega \cdot \text{cm})^{-1}$) for other materials.

Materials	σ_{CSH}	σ_{MSH}	σ_{SAH}
Nonmagnets			
Pt	4324 [23]	0	0
W	2540 [45]	0	0
Ta	631 [46]	0	0
Antiferromagnets			
Mn ₂ Au	541.16 [47]	0.04 [47]	
Ferromagnets			
Fe	241.52 [47]	5.74 [47]	-838 [16]
L10 FePt	324 [17]		564 [17]
A1 FePt	1195	788	159
(this work)			

APPENDIX C: MAGNETIC RASHBA MODEL

The spin Hall conductivity can also be evaluated from the eigenstates of a system by decomposing spin Hall conductivity into *T*-even and *T*-odd contributions as follows [48]:

$$\sigma_{\mu\nu}^{\xi, \text{even}} = -\frac{\hbar}{V} \sum_{n,m,k} (f_{mk} - f_{nk}) \frac{\text{Im}(\langle n | \hat{J}_{k,\mu}^{\xi} | m \rangle \langle m | \hat{J}_{k,\nu} | n \rangle)}{(\varepsilon_{nk} - \varepsilon_{mk})^2 + (\hbar\Gamma)^2}, \quad (\text{C1a})$$

$$\sigma_{\mu\nu}^{\xi, \text{odd}} = \frac{\hbar^2\Gamma}{V} \sum_{n,m,k} \frac{f_{mk} - f_{nk}}{\varepsilon_{nk} - \varepsilon_{mk}} \frac{\text{Re}(\langle n | \hat{J}_{k,\mu}^{\xi} | m \rangle \langle m | \hat{J}_{k,\nu} | n \rangle)}{(\varepsilon_{nk} - \varepsilon_{mk})^2 + (\hbar\Gamma)^2}, \quad (\text{C1b})$$

where $f_{nk} = \frac{1}{1+e^{\beta(\varepsilon_{nk}-\varepsilon_F)}}$ is the Fermi-Dirac distribution, $\hat{J}_{k,\nu} = -e\hat{v}_{k,\nu} = -e\hbar^{-1} \frac{\partial H_k}{\partial k_{\nu}}$, and $\hat{J}_{k,\mu}^{\xi}$ represents the electric- and spin current operators, respectively. $\hat{v}_{k,\mu}$ is the velocity operator and $\hbar\Gamma$ is an artificial energy broadening by taking into account the electron scattering and finite lifetime.

The *T*-even and *T*-odd spin Hall conductivity can be further decomposed into intraband ($m = n$) and interband ($m \neq n$) contributions. The *T*-even spin Hall conductivity $\sigma_{\mu\nu}^{\xi, \text{even}}$, such as conventional and spin anomalous Hall conductivity for

ferromagnets, only has interband contribution. And, in the clean limit $\Gamma \rightarrow 0$, it can be calculated by spin Berry curvature as follows:

$$\sigma_{\mu\nu}^{\xi, \text{even}(\text{inter})} = \frac{e\hbar}{V} \sum_{n \neq m, k} (f_{mk} - f_{nk}) \frac{\text{Im}(\langle n | \hat{J}_{k,\mu}^{\xi} | m \rangle \langle m | \hat{v}_{k,\nu} | n \rangle)}{(\varepsilon_{nk} - \varepsilon_{mk})^2}. \quad (\text{C2})$$

The *T*-odd spin Hall conductivity $\sigma_{\mu\nu}^{\xi, \text{odd}}$, i.e., magnetic spin Hall conductivity for ferromagnets, in the almost clean limit, is mainly contributed by the intraband ($m = n$) transition [20]:

$$\sigma_{\mu\nu}^{\xi, \text{odd}(\text{intra})} = \frac{-e}{\Gamma V} \sum_{n,k} \langle n | \hat{J}_{k,\mu}^{\xi} | n \rangle \langle n | \hat{v}_{k,\nu} | n \rangle \left(-\frac{\partial f_{nk}}{\partial \varepsilon} \right) \quad (\text{C3})$$

It is worth noting that *T*-odd spin Hall conductivity $\sigma_{\mu\nu}^{\xi, \text{odd}}$ is proportional to $1/\Gamma$ and will diverge in the clean limit $\Gamma \rightarrow 0$.

As shown in Fig. 6, we employ Rashba models that are applicable for systems without inversion symmetry to have an intuitive understanding on the general features of various spin Hall mechanisms in magnetic systems. The case 1 is the standard Rashba model without magnetization [49]

$$H_0 = \frac{\hbar^2}{2m} k^2 + \alpha(k_y\sigma_x - k_x\sigma_y) \quad (\text{C4})$$

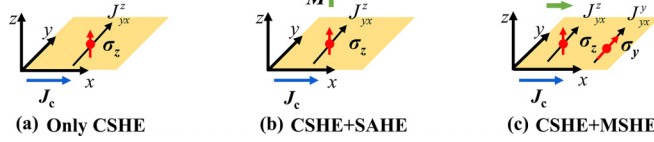


FIG. 6. The schematic diagrams of spin Hall effect for Rashba models. The directions of charge current J_c , the magnetization M , and spin current J_s have been marked in blue, green, and black arrows, respectively. The spin polarization σ of the spin current has been shown in red.

where m is the electron effective mass, α is the Rashba parameter, and $\sigma_{x,y}$ are the Pauli matrices. In this case, there is only conventional spin Hall effect. The spin Hall conductivity can be calculated based on Eq. (C2):

$$\sigma_{yx}^z = \frac{e\hbar^2}{16\pi m\alpha} (k_F^- - k_F^+) = \frac{e}{8\pi} \quad (\text{C5})$$

where k_F^+ and k_F^- indicate the Fermi wave vector for two branches.

Case 2 as shown in Fig. 6(b) is the magnetic Rashba model with out-of-plane magnetization, which may be realized at “nonmagnetic metal/ferromagnetic insulator with out-of-plane magnetization” interface:

$$H_0 = \frac{\hbar^2}{2m} k^2 + \alpha(k_y\sigma_x - k_x\sigma_y) - J\sigma_z \quad (\text{C6})$$

where J represents the proximity magnetic exchange energy. In this case, there is conventional spin Hall as well as spin anomalous Hall effect. The eigenstates of the above out-of-plane magnetic Rashba model are

$$\varepsilon_k^\pm = \frac{\hbar^2}{2m} k^2 \pm \sqrt{J^2 + (\alpha k)^2} \quad (\text{C7})$$

$$|\psi_k^+\rangle = \begin{pmatrix} i \sin \frac{\theta}{2} \\ e^{i\phi} \cos \frac{\theta}{2} \end{pmatrix}, \quad |\psi_k^-\rangle = \begin{pmatrix} -i \cos \frac{\theta}{2} \\ e^{i\phi} \sin \frac{\theta}{2} \end{pmatrix}, \quad (\text{C8})$$

where $\cos \theta = J/\sqrt{J^2 + (\alpha k)^2}$, $k_x = k \cos \phi$, and $k_y = k \sin \phi$.

According to Eq. (C2), the spin Hall conductivity can be calculated as

$$\begin{aligned} \sigma_{yx}^z &= \frac{e\hbar}{V} \sum_{n \neq m, k} (f_{mk} - f_{nk}) \frac{\text{Im}(\langle n | \hat{J}_{s,y}^z | m \rangle \langle m | \hat{v}_x | n \rangle)}{(\varepsilon_{nk} - \varepsilon_{mk})^2} \\ &= \frac{2e\hbar}{(2\pi)^2} \int_{k_F^+}^{k_F^-} k dk \int_0^{2\pi} d\phi \\ &\quad \times \text{Im} \frac{-\frac{\hbar^2}{2m} \sin \theta k_y \times (-i\frac{\alpha}{\hbar} \sin \phi - \frac{\alpha}{\hbar} \cos \phi \cos \theta)}{4(J^2 + \alpha^2 k^2)} \\ &= \frac{e\hbar^2}{16\pi m\alpha^2} \left(\sqrt{J^2 + \alpha^2 k^2} + \frac{J^2}{\sqrt{J^2 + \alpha^2 k^2}} \right) \Big|_{k_F^+}^{k_F^-} \quad (\text{C9}) \end{aligned}$$

where k_F^+ and k_F^- indicate the Fermi wave vector for two branches. One can clearly observe that the spin Hall conductivity is a function of J^2 , which is T -even as expected.

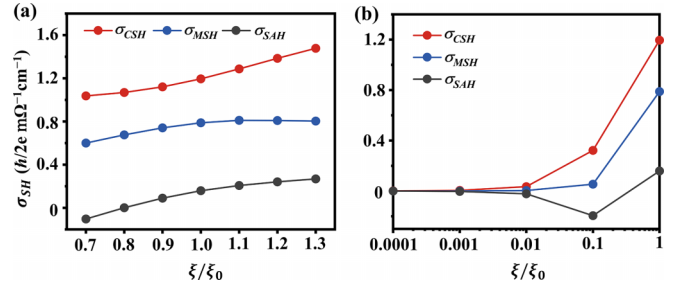


FIG. 7. The conventional (red), magnetic (blue), and spin anomalous Hall conductivity (black) as a function of the SOC strength ξ/ξ_0 . The result at nonrelativistic limit is shown on the left ($\xi/\xi_0 \rightarrow 0$) in (b).

Case 3 as shown in Fig. 6(c) is the magnetic Rashba model with in-plane magnetization, which may be realized at “nonmagnetic metal/ferromagnetic insulator with in-plane magnetization” interface:

$$H_0 = \frac{\hbar^2}{2m} k^2 + \alpha(k_y\sigma_x - k_x\sigma_y) - J\sigma_x \quad (\text{C10})$$

In this case, there is conventional spin Hall as well as magnetic spin Hall effect. When the electric current is along the x direction, the transverse spin current generated by MSHE will flow along the y direction with σ_y spin polarization.

The eigenstates of the above Hamiltonian are

$$\varepsilon_k^\pm = \frac{\hbar^2}{2m} k^2 \pm \sqrt{J^2 + (\alpha k)^2 - 2J\alpha k_y}, \quad (\text{C11})$$

$$|\psi_k^+\rangle = \frac{1}{\sqrt{2}} \begin{pmatrix} \frac{\sqrt{(J^2 - 2J\alpha k_y + k^2\alpha^2)}}{(J + i\alpha k e^{i\phi})} \\ 1 \end{pmatrix}. \quad (\text{C12})$$

The corresponding magnetic spin Hall conductivity σ_{yx}^y can be calculated based on Eq. (C2) as

$$\begin{aligned} \sigma_{yx}^y &= \frac{-e}{\Gamma V} \sum_{n,k} \langle n | J_{s,y}^y | n \rangle \langle n | v_x | n \rangle \left(-\frac{\partial f_{nk}}{\partial \varepsilon} \right) \\ &= \frac{e}{4\Gamma\pi^2} \sum_{\delta=\pm} k_F^\delta \int_0^{2\pi} \\ &\quad \times \left[\frac{\hbar(\alpha k_F^\delta)^3 \cos^2 \phi \sin \phi}{2m[J^2 + (k_F^\delta)^2 \alpha^2 - 2J(\alpha k_F^\delta) \sin \phi]} \right. \\ &\quad \left. - \frac{J\hbar^3 k_x^2 k_y^2 \alpha^2}{2m^2(J^2 + k^2 \alpha^2)^{3/2}} \right] d\phi \\ &\approx \frac{e\hbar}{32\pi m\Gamma} \sum_{\delta=\pm} \left[J(k_F^\delta) + \frac{\alpha^4 (k_F^\delta)^5}{J^3} \right. \\ &\quad \left. - \frac{\hbar^2 J \alpha^2 (k_F^\delta)^5}{m[J^2 + (\alpha k_F^\delta)^2]^{3/2}} \right]. \quad (\text{C13}) \end{aligned}$$

In order to obtain the above analytical expression of σ_{yx}^y , we assume $J \ll k$ and ignore $J\alpha k_y$ in the energy-band dispersion. One can observe that the magnetic spin Hall conductivity is a function of J and J^3 , which is T -odd as expected. Meanwhile,

the corresponding longitudinal electric conductivity can be calculated as

$$\begin{aligned}\sigma_{xx} &= \frac{e^2}{\Gamma} \sum_{n,k} \langle n|v_x|n\rangle \langle n|v_x|n\rangle \\ &= \frac{4e^2\pi}{\Gamma} \sum_{\delta=\pm} (k_F^\delta)^3 \left[\frac{\hbar^2}{m^2} + \frac{\alpha^4}{\hbar^2[J^2 + (\alpha k_F^\delta)^2]} \right].\end{aligned}\quad (\text{C14})$$

It can be seen that both σ_{yx}^y and σ_{xx} are proportional to $1/\Gamma$; in consequence, the magnetic spin Hall angle $\theta_{\text{MSH}} = \sigma_{yx}^y/\sigma_{xx}$ will not depend on Γ .

APPENDIX D: THE DEPENDENCE OF SPIN HALL EFFECT ON SPIN-ORBIT COUPLING

Figure 7 shows the spin Hall conductivities as a function of SOC strength (ξ/ξ_0). One can see that all three types of spin Hall conductivities are proportional to the SOC strength, and vanish at the limit $\xi/\xi_0 \rightarrow 0$.

APPENDIX E: THE SPIN THz EMISSION IN SINGLE-LAYER FERROMAGNET

Similar to the model of ferromagnet/nonmagnet bilayers [38,50], the emitted THz electric field in a single-layer ferromagnet can be described as

$$E_{\text{THz}} = \frac{P_{\text{abs}}}{d_{\text{FM}}} \lambda_{\text{FM}} \tanh\left(\frac{d_{\text{FM}}}{2\lambda_{\text{FM}}}\right) \theta \frac{1}{n_{\text{air}} + n_{\text{sub}} + Z_0(\sigma_{\text{FM}}d_{\text{FM}})},\quad (\text{E1})$$

where P_{abs} indicates pump-pulse absorbency, d_{FM} is the thickness of FM layer, and λ_{FM} is relaxation length, which depends on materials and frequency. θ represents the total spin Hall angle originating from multiple spin Hall mechanisms. n_{air} and n_{sub} are the refractive indices in air and substrate, Z_0 is the impedance of vacuum, and σ_{FM} is the electrical conductivity. The first term indicates absorption of the optical pump pulse, the second term denotes spin diffusion in FM layer, and the third term represents spin-to-charge conversion, as well as the last term, which shows that the charge current acts as a source of a THz electromagnetic pulse. From the above equation, one can find that the efficiency of the THz emitter is proportional to spin Hall angle.

-
- [1] J. Sinova, S. O. Valenzuela, J. Wunderlich, C. H. Back, and T. Jungwirth, Spin Hall effect, *Rev. Mod. Phys.* **87**, 1213 (2015).
- [2] A. Hoffmann, Spin Hall effects in metals, *IEEE Trans. Magn.* **49**, 5172 (2013).
- [3] L. Liu, O. J. Lee, T. J. Gudmundsen, D. C. Ralph, and R. A. Buhrman, Current-induced switching of perpendicularly magnetized magnetic layers using spin torque from the spin Hall effect, *Phys. Rev. Lett.* **109**, 096602 (2012).
- [4] A. Manchon, J. Železný, I. M. Miron, T. Jungwirth, J. Sinova, A. Thiaville, K. Garello, and P. Gambardella, Current-induced spin-orbit torques in ferromagnetic and antiferromagnetic systems, *Rev. Mod. Phys.* **91**, 035004 (2019).
- [5] X. Han, X. Wang, C. Wan, G. Yu, and X. Lv, Spin-orbit torques: Materials, physics, and devices, *Appl. Phys. Lett.* **118**, 120502 (2021).
- [6] Q. Shao *et al.*, Roadmap of spin-orbit torques, *IEEE Trans. Magn.* **57**, 1 (2021).
- [7] B. F. Miao, S. Y. Huang, D. Qu, and C. L. Chien, Inverse spin Hall effect in a ferromagnetic metal, *Phys. Rev. Lett.* **111**, 066602 (2013).
- [8] N. Nagaosa, J. Sinova, S. Onoda, A. H. MacDonald, and N. P. Ong, Anomalous Hall effect, *Rev. Mod. Phys.* **82**, 1539 (2010).
- [9] T. Taniguchi, J. Grollier, and M. D. Stiles, Spin-transfer torques generated by the anomalous Hall effect and anisotropic magnetoresistance, *Phys. Rev. Appl.* **3**, 044001 (2015).
- [10] S. Iihama, T. Taniguchi, K. Yakushiji, A. Fukushima, Y. Shiota, S. Tsunegi, R. Hiramatsu, S. Yuasa, Y. Suzuki, and H. Kubota, Spin-transfer torque induced by the spin anomalous Hall effect, *Nat. Electron.* **1**, 120 (2018).
- [11] J. D. Gibbons, D. MacNeill, R. A. Buhrman, and D. C. Ralph, Reorientable spin direction for spin current produced by the anomalous Hall effect, *Phys. Rev. Appl.* **9**, 064033 (2018).
- [12] T. Seki, S. Iihama, T. Taniguchi, and K. Takanashi, Large spin anomalous Hall effect in $\text{Li}_0\text{-FePt}$: Symmetry and magnetization switching, *Phys. Rev. B* **100**, 144427 (2019).
- [13] S. C. Baek, V. P. Amin, Y. Oh, G. Go, S.-J. Lee, M. D. Stiles, B.-G. Park, and K.-J. Lee, Spin currents and spin-orbit torques in ferromagnetic trilayers, *Nat. Mater.* **17**, 509 (2018).
- [14] H. Wu, S. A. Razavi, Q. Shao, X. Li, K. L. Wong, Y. Liu, G. Yin, and K. L. Wang, Spin-orbit torque from a ferromagnetic metal, *Phys. Rev. B* **99**, 184403 (2019).
- [15] T. Y. Ma, C. H. Wan, X. Wang, W. L. Yang, C. Y. Guo, C. Fang, M. K. Zhao, J. Dong, Y. Zhang, and X. F. Han, Evidence of magnetization switching by anomalous spin Hall torque in NiFe, *Phys. Rev. B* **101**, 134417 (2020).
- [16] V. P. Amin, J. Li, M. D. Stiles, and P. M. Haney, Intrinsic spin currents in ferromagnets, *Phys. Rev. B* **99**, 220405(R) (2019).
- [17] Y. Miura and K. Masuda, First-principles calculations on the spin anomalous Hall effect of ferromagnetic alloys, *Phys. Rev. Mater.* **5**, L101402 (2021).
- [18] M. Seemann, D. Kodderitzsch, S. Wimmer, and H. Ebert, Symmetry-imposed shape of linear response tensors, *Phys. Rev. B* **92**, 155138 (2015).
- [19] X. R. Wang, Anomalous spin Hall and inverse spin Hall effects in magnetic systems, *Commun. Phys.* **4**, 55 (2021).
- [20] A. Mook, R. R. Neumann, A. Johansson, J. Henk, and I. Mertig, Origin of the magnetic spin Hall effect: Spin current vorticity in the Fermi sea, *Phys. Rev. Res.* **2**, 023065 (2020).
- [21] L. Salemi and P. M. Oppeneer, Theory of magnetic spin and orbital Hall and Nernst effects in bulk ferromagnets, *Phys. Rev. B* **106**, 024410 (2022).
- [22] M. Kimata, H. Chen, K. Kondou, S. Sugimoto, P. K. Muduli, M. Ikhlas, Y. Otori, T. Tomita, A. H. MacDonald, S. Nakatsuji, and Y. Otani, Magnetic and magnetic inverse spin Hall effects

- in a non-collinear antiferromagnet, *Nature (London)* **565**, 627 (2019).
- [23] D. Ködderitzsch, K. Chadova, and H. Ebert, Linear response Kubo-Bastin formalism with application to the anomalous and spin Hall effects: A first-principles approach, *Phys. Rev. B* **92**, 184415 (2015).
- [24] H. Ebert *et al.*, The Munich SPR-KKR Package, version 8.6, <http://olymp.cup.uni-muenchen.de/ak/ebert/sprkr> (2017).
- [25] H. Ebert, D. Ködderitzsch, and J. Minár, Calculating condensed matter properties using the KKR-Green's function method—recent developments and applications, *Rep. Prog. Phys.* **74**, 096501 (2011).
- [26] S. H. Vosko, L. Wilk, and M. Nusair, Accurate spin-dependent electron liquid correlation energies for local spin density calculations: A critical analysis, *Can. J. Phys.* **58**, 1200 (1980).
- [27] B. Velický, Theory of electronic transport in disordered binary alloys: Coherent-potential approximation, *Phys. Rev.* **184**, 614 (1969).
- [28] W. H. Butler, Theory of electronic transport in random alloys: Korringa-Kohn-Rostoker coherent-potential approximation, *Phys. Rev. B* **31**, 3260 (1985).
- [29] I. Turek, J. Kudrnovský, V. Drchal, L. Szunyogh, and P. Weinberger, Interatomic electron transport by semiempirical and *ab initio* tight-binding approaches, *Phys. Rev. B* **65**, 125101 (2002).
- [30] S. Lowitzer, D. Ködderitzsch, and H. Ebert, Coherent description of the intrinsic and extrinsic anomalous Hall effect in disordered alloys on an *ab initio* level, *Phys. Rev. Lett.* **105**, 266604 (2010).
- [31] J. Shi, P. Zhang, D. Xiao, and Q. Niu, Proper definition of spin current in spin-orbit coupled systems, *Phys. Rev. Lett.* **96**, 076604 (2006).
- [32] D. Monaco and L. Ulčakar, Spin Hall conductivity in insulators with nonconserved spin, *Phys. Rev. B* **102**, 125138 (2020).
- [33] F. Mahfouzi and N. Kioussis, Elastodynamically induced spin and charge pumping in bulk heavy metals, *Phys. Rev. Lett.* **128**, 215902 (2022).
- [34] H. Ebert, S. Mankovsky, K. Chadova, S. Polesya, J. Minár, and D. Ködderitzsch, Calculating linear-response functions for finite temperatures on the basis of the alloy analogy model, *Phys. Rev. B* **91**, 165132 (2015).
- [35] J. Ryu, R. Thompson, J. Y. Park *et al.*, Efficient spin-orbit torque in magnetic trilayers using all three polarizations of a spin current, *Nat. Electron.* **5**, 217 (2022).
- [36] N. Soya, M. Yamada, K. Hamaya, and K. Ando, Isotropic spin Hall effect in an epitaxial ferromagnet, *Phys. Rev. Lett.* **131**, 076702 (2023).
- [37] E. Papaioannou and R. Beigang, THz spintronic emitters: A review on achievements and future challenges, *Nanophotonics* **10**, 1243 (2021).
- [38] T. S. Seifert, L. Cheng, Z. X. Wei, T. Kampfrath, and J. B. Qi, Spintronic sources of ultrashort terahertz electromagnetic pulses, *Appl. Phys. Lett.* **120**, 180401 (2022).
- [39] M. Y. Tong, Y. Z. Hu, W. B. He, S. Y. Hu, X. Cheng, and T. Jiang, Light-driven spintronic heterostructures for coded terahertz emission, *ACS Nano* **16**, 8294 (2022).
- [40] L. Zhu, D. C. Ralph, and R. A. Buhrman, Unveiling the mechanism of bulk spin-orbit torques within chemically disordered $\text{Fe}_x\text{Pt}_{1-x}$ single layer, *Adv. Funct. Mater.* **31**, 2103898 (2021).
- [41] S. U. Jen, T. P. Chen, and B. L. Chao, Saturation moment, specific heat, and transport properties of disordered $\text{Co}_{100-x}\text{Pt}_x$ alloys, *Phys. Rev. B* **48**, 12789 (1993).
- [42] T. R. McGuire, J. A. Aboaf, and E. Klokholm, Magnetic and transport properties of Co-Pt thin films, *J. Appl. Phys.* **55**, 1951 (1984).
- [43] I. Turek, J. Kudrnovský, and V. Drchal, *Ab initio* theory of galvanomagnetic phenomena in ferromagnetic metals and disordered alloys, *Phys. Rev. B* **86**, 014405 (2012).
- [44] O. Jaoul, I. A. Campbell, and A. Fert, Spontaneous resistivity anisotropy in Ni alloys, *J. Magn. Magn. Mater.* **5**, 23 (1977).
- [45] W. Zhang, W. Han, X. Jiang, S.-H. Yang, and S. S. P. Parkin, Role of transparency of platinum-ferromagnet interfaces in determining the intrinsic magnitude of the spin Hall effect, *Nat. Phys.* **11**, 496 (2015).
- [46] L. Liu, C. F. Pai, Y. Li, H. W. Tseng, D. C. Ralph, and R. A. Buhrman, Spin-torque switching with the giant spin Hall effect of Tantalum, *Science* **336**, 555 (2012).
- [47] P. Li, J. Z. Zhang, Z. X. Guo, T. Min, and X. Wang, Intrinsic anomalous spin Hall effect, *Sci. China-Phys. Mech. Astron.* **66**, 227511 (2023).
- [48] J. Železný, Y. Zhang, C. Felser, and B. Yan, Spin-polarized current in noncollinear antiferromagnets, *Phys. Rev. Lett.* **119**, 187204 (2017).
- [49] Y. A. Bychkov and E. I. Rashba, Oscillatory effects and the magnetic susceptibility of carriers in inversion layers, *J. Phys. C: Solid State Phys.* **17**, 6039 (1984).
- [50] G. Torosyan, S. Keller, L. Scheuer, R. Beigang, and E. T. Papaioannou, Optimized spintronic terahertz emitters based on epitaxial grown Fe/Pt layer structures, *Sci. Rep.* **8**, 1311 (2018).